

EXPERIMENTAL ANALYSIS OF THE SPATIAL AND TEMPORAL FLUCTUATIONS IN A CAVITATING WATER JET

S.A. Campbell, C.A. Fairfield
Napier University
Edinburgh, Scotland, U.K.

ABSTRACT

The application of experimental techniques to analyse the physical behaviour of a cavitating water jet at pressures up to 10000 psi (68.95 MNm^{-2}) and flow rates up to 10.81 gallons (U.S.) *per* minute ($6.82 \times 10^{-4} \text{ m}^3\text{s}^{-1}$) is described. In British civil engineering practice, this range of pressures and flow rates covers that used in the routine cleaning and maintenance of drains or sewers, graffiti removal, and hydraulic pick excavation on soft soils. The techniques used were: high-speed video image analysis at 20000 frames *per* second, thermal image analysis of the nozzle, *vena contracta* and divergent jet, spectral analysis followed by fast Fourier transform analysis of the vibrations encountered in the system, and laser scattering analysis for spray droplet or bubble sizing in the jet. Correlations between the measured dynamic responses in the jet and the observed cyclic pressure fluctuations were drawn. Temporal and spatial variations in the jet's shape and size were measured and also related to these fluctuations. The jet was illuminated by coherent pulsed laser: the subsequent Mie scattering of the light was related to the size of bubbles, spray droplets, and the cavitation nuclei forming in the jet. Subsequent work uses this physical characterisation of the jet to evaluate the damage to a range of typical drains and sewer materials.

1 INTRODUCTION

Following on from earlier research by the authors^[1-3], this current work sets out to investigate the physical and thermal properties of high-pressure water jetting equipment which bear upon the ability of thermoplastic and ceramic pipe-wall materials to resist the damage imparted by the jet when used to clean and unblock sewers.

Elaborating on the work of Kobayashi and Ito^[4] and Soyama *et al.*^[5], high-speed video image analysis was carried out on the jet, under a range of conditions. Sequential analysis of a series of 5×10^{-5} s time interval frames was carried out. This enabled detailed examination of the different zones of the jet and aided accurate jet characterisation in terms of the periodic spatial and temporal fluctuations along its length.

Cavitating bubbles have been shown to release heat energy^[6], therefore thermal image analysis of the nozzle and the exiting jet was carried out. Thermal images of the jet at a range of different pressures were captured. Analyses of these images facilitated verification of whether localised regions of relatively high temperatures were present in the jet. Global temperature distributions across the width of the jet as well as along its length were also measured to examine the effect of the cooler ambient temperature upon the relatively hot jet.

Accelerometers coupled to a front-end spectrum analyser were used to measure the magnitude of acceleration (and hence vibration) of the nozzle and pumphead of the high-pressure water jetting system, under a range of conditions. Time domain plots were obtained, to which fast Fourier transforms (FFTs) were applied to yield frequency domain plots that enabled extraction of the fundamental frequencies of the nozzle and pumphead. The dynamic responses from the spectral analyses were correlated with the frequencies of the pressure fluctuations in the system; a 5 ms response time pressure transducer was used to record pressure *versus* time traces, from which the frequency and magnitude of any fluctuations were recorded.

As cavitation is the main damage instigator in liquid-solid impact at the pressures used herein^[7,8], coherent pulsed laser diode techniques were employed using Mie scattering and laser diffraction methods, to assess the size distributions of bubbles and droplets in the flow. Sizes measured were analysed to assess the probability of getting any given bubble size for a range of pressures. The bubble sizes measured agreed with established values^[7].

2 EXPERIMENTAL DETAILS

This section explains the experimental techniques of the basic jetting equipment, through to the analyses carried out on the results obtained from the subsequent experiments.

2.1 Jetting apparatus

A positive displacement plunger pump was used to deliver the pressures and flow rates needed. The unit used was a Hughes 1000 series with a 26 mm plunger. It was powered by a 6000 cm³ (non-turbo) Type 6354 Perkins engine which delivered 120 hp (89.5 kW). It was fed with mains

water by a stand-pipe and 63.5 mm internal diameter high-tensile polyvinylchloride/rubber nitrile hose. The influx of water to the header tank on the low-pressure side of the pump was controlled using a ballcock. This pumping system fed the jetting rig, which can be seen in Figure 1. The safety cage for the rig was manufactured from Dexion framework and wire mesh. Safe operation of the rig was imperative as the water pressures used herein can be extremely dangerous^[9].

2.2 Pressure monitoring

To ensure the reliability of the readings on the pressure gauge, an electronic pressure transducer was plumbed into the system, in parallel with the stainless steel lance. The unit used was a Gems 5 ms response time transducer. The readings from the transducer were logged to a PC through the auxiliary channel of a Brüel & Kjær PULSE system spectrum analyser. The transducer's output signal range was 0 – 5 V, which corresponded to 0 – 1000 bar (0 – 14500 psi or 100 MPa). The change in pressure caused the diaphragm in the transducer to expand or contract which in turn sent a voltage signal to the data logger. Post-processing enabled these voltage readings to be converted to pressures, which enabled pressure *versus* time traces for a range of pressures to be measured and recorded. Figure 2 shows a schematic of the pressure transducer set-up.

2.3 High-speed video imaging

The high-speed video imaging was carried out using a NAC Systems Memrecam RX-6 video camera. The experimental set-up can be seen in Figure 3. The frame rate and shutter speed were set to 20000 frames *per* second and 10^{-5} s respectively. This high frame rate (approximately 800 times faster than a standard U.K. television) ensured that the fluctuations along the jet's length were captured at as small a time interval as possible, hence enhancing the video representation of the aforementioned fluctuations. The jet was imaged while running at a range of pressures. The shutter speed enabled the optimum amount of light into the camera whilst illuminating the jet; the series of photographs taken from the video footage shown in Figure 4 showed a strong contrast between the jet and the background.

2.4 Thermal image analysis

The camera was calibrated using a matt black plate of known emissivity and of uniform temperature; 15 temperature measurements were taken with a thermocouple and hand-held logger, covering the surface of the plate. The nozzle was also painted matt black to facilitate a constant emissivity field of view when looking through the camera's viewfinder so that when the jet began to issue into atmosphere it acted as an object of different temperature contrast thus allowing the level (this set the temperature range to be measured) and sensitivity (this fine-tuned within the range set by the level control) of the camera to be optimised. The jet was imaged running at a range of pressures for two minutes, and recorded onto a Hi-8 tape; the Hi-8 recorder also incorporated a monitor on which real-time thermal image footage could be viewed whilst the jet was running. The footage was imported into a PC using a data capture card and subsequent analysis involved investigating the global temperature change between pressures and also the temperature change as a function of time for a given pressure. A schematic view of the thermal imaging set-up can be seen in Figure 5.

2.5 Spectral analysis

The aforementioned Brüel & Kjær PULSE system spectrum analyser was used to measure and record the dynamic responses from different parts of the jetting system at the range of target pressures stated. An accelerometer was attached, using a beeswax couplant, to both the nozzle and the pumphead and the responses measured under a range of conditions. Background readings were recorded to establish a control, then the responses were recorded with an HGV passing within 10 m of the jetting rig at approximately 10 mph. Thereafter, readings were taken at a range of throttle settings (idling, mid-range and full), then finally at a range of pressures with the engine running at full throttle (2200 rpm). The PULSE system recorded the dynamic responses as a series of acceleration *versus* time traces. An FFT was applied to said plots to yield frequency domain plots. The fundamental (resonant) frequencies were derived therefrom and correlated to the measured fluctuations in the jet, described in Section 2.3. Figure 6 shows the set-up of the spectral analysis equipment.

2.6 Jet bubble size analysis

A Malvern Instruments Spraytec was used to gauge the size of particles in the jet. The method involved shining a pulsed diode laser through the jet; using a combination of laser diffraction and Mie scattering, the software on the Spraytec PC was able to calculate the sizes of the particles in the flow. The Spraytec was fitted with a lens which was able to resolve bubbles up to 600 μm in diameter. Figure 7 shows Spraytec set-up.

3 RESULTS

Figures 8, and later Figures 12 to 15, show the fluctuations monitored over a *c.* 20 s period with the first fundamental frequency, f_0 stated thereon. The sampling rate of the pressure measurements was 5 ms; this satisfied the Nyquist criterion, thus avoiding aliasing errors. The pressure was recorded from when the valve on the high-pressure line was opened until it was closed, hence the “run-up” and “run-down” times were included in the recording, of which *c.* 10 s was live test time at the desired pressure. Figure 9 shows the discretised digital signal output from the pressure transducer over the 8000 ms to 12000 ms window. By expanding the x-axis as in Figure 10, the trace becomes more like a continuous signal, which lends itself to FFT analysis; indeed, the FFT output of this signal can be seen in Figure 11. Figure 16 shows the fluctuations for all pressures (including the run-up and run-down times) together for comparison.

Looking again at the series of still images in Figure 4, the spatial fluctuations in the size and shape of the jet are clear, even with frames as short as 5×10^{-5} s. These are indicative of the nature of the fluctuations recorded in the jet, for all of the target pressures used. Two minutes of footage was recorded for each pressure and stored to DVD. The high frame rate meant that the resolution of the video was small in comparison with other movie files, such as .mpeg or .avi formats.

Figures 17 shows still images captured from the thermal imaging footage of the jet. These images show the jet issuing into atmosphere from the nozzle. These images are indicative of the

footage obtained. The temperatures measured in the jet increased as the pressure increased. Localised regions of relatively higher temperature were found; the nozzle was consistently hotter than the lance *and* the jet.

Figures 18 and 19 show the time domain plot and the resulting frequency domain plot respectively, for the pumphead; Figures 20 and 21 show the same plots for the nozzle. These were indicative of the nature of the time and frequency domain plots obtained for all the target pressures used. As mentioned, the frequency domain plots were obtained by applying an FFT to the time domain plot. Equation 1 shows the general form of FFT, $F\{f(t)\}$ used to transform periodic time domain plots, $f(t)$ into frequency domain plots.

$$F\{f(t)\} = \int_{-\infty}^{\infty} f(t)e^{-jt\omega} dt \quad \text{Eq. 1}$$

Where ω is angular velocity in rad.s^{-1} and t is time in s. The Brüel & Kjær PULSE system spectrum analyser used a Hanning weighting function, w , (sometimes referred to as a Hanning window; the general form of a Hanning window is given in Equation 2).

$$w(t) = \cos 2\pi t/T \quad \text{Eq. 2}$$

Where t is time in s, and T is the period of the function, also in s.

Table 1 shows the comparison between the first fundamental frequencies of the measured pressure fluctuations and the first fundamental frequencies of the vibrations of the pumphead and nozzle.

Figures 22 and 23 show the results of the laser measured jet bubble size. Figure 22 shows a basic grading curve for each pressure and Figure 23 shows the frequency of bubble size occurrence, as a percentage of the total number of bubbles measured, for each pressure. Photometric analysis of the mains water used in the jetting tests showed $< 1 \text{ mgdm}^{-3}$ suspended solids content, it was fair to assume that the results pertained to either cavities or droplets in the flow or spray zones.

4 DISCUSSION

It should be borne in mind that the jetting equipment used for this research was not a unit typically used in advanced research laboratories; it was a diesel-operated industrial pump, typical of that used in the U.K for cleaning and unblocking sewers.

It is clear from Table 1 that there was no relationship between the frequencies of vibration of the pumphead and nozzle and the pressure fluctuations. This implies that there was another driving force behind these fluctuations; Figures 8 and 12 to 15 show that these fluctuations were not random. The FFT analysis showed that 97.47% of the energy used to cause the pressure to fluctuate was of low frequency (between 2.25 Hz and 4.25 Hz), which agreed with the non-correlation between it and the vibrations of the nozzle and pumphead as their first fundamental frequencies were much higher.

The pressure was also recorded at a sampling interval of 1 s, but these data were not used for two reasons:

1. They did not satisfy the Nyquist criterion.
2. Even if they did, they were too slow to capture those fluctuations occurring at frequencies greater than 1 Hz which, as can be seen in Figures 8, and 12 to 15, were prominent.

The spectral measurements of the pumthead at 8000 psi (55.2 MPa) and 10000 psi (69.0 MPa), were erroneous when post-processed. The likely reason for this was overloading of the accelerometer. Looking at Table 1, it can be seen that the first fundamental frequency of the nozzle at 8000 psi was 155.2 Hz (49.80%) higher than the mean for all the other pressures.

The results from thermal image analysis showed that there were no localised regions of relatively higher temperatures in the jet for all target pressures; the heat emission of approximately 15000 K brought about by the adiabatic bubble collapse only lasts between 100 ps and 300 ps^[10]. This event was too short for the camera to capture and the accompanying temperature rise and subsequent dissipation of heat too rapid.

The temperature rise with increasing pressure of the flow was expected; as the flow approached the nozzle, the outer streamlines of the flow were frictionally heated by the inside of the lance, this temperature increase was a function of pressure, therefore it was also a function of the velocity. Similarly, when the jet became open to atmosphere, the outer streamlines were frictionally heated by the surrounding air. Although the short duration pulses of heat arising from cavitation were not detected, some of the general temperature increase above the 278.7 K (5.7°C) ambient water temperature may have been due to cavitation.

The jet bubble analysis yielded interesting results; Figure 23 shows that for all particle diameters up to approximately 20 µm, the pressures were ranked in descending order; the percentage, of any given particle diameter, of the total number of particles was larger for higher pressures and lower for lower pressures. Between 20 µm and 30 µm, these roles were reversed and now the opposite was true for all remaining particles. This is an area of the jet bubble analysis that merits future research; finding out what happens to particles as they reach the range 20 µm to 30 µm is the next step. Figure 22 shows a typical grading curve for the measured particle diameters. As would be expected, they all appear in rank order, converging as they approach 100%.

The high-speed video image analysis showed the high frequency of spatial fluctuations in the jet, at least 20 kHz. This frequency was governed by the frame rate of the camera; it was impossible to freeze the jet, but using helium driven cameras that can operate up to 100 MHz (*i.e.* an interval of 100 ns between each frame) would serve to compare the observed frequencies.

5 CONCLUSIONS

- There was no relationship between the frequencies of vibration of the pumphead and nozzle and the pressure fluctuations at the lance.
- Jet temperature increased with jet pressure, with a 7.4 K increase recorded over the full range of pressures (*i.e.* between 2000 psi (13.8 MPa) and 10000 psi (69.0 MPa)).
- There were no localised regions of relatively higher temperatures in the jet, at any pressure, although the nozzle itself exhibited a 5.1×10^{-2} K temperature increase *per* MPa.
- The jet showed signs of extreme spatial fluctuation at least every 5×10^{-5} s.
- The bubble size analysis showed there were bubbles in the flow, therefore cavitation will occur due to the pressure drop.

6 ACKNOWLEDGEMENT

The authors thank the following people for their help:

Mr Iain Swan, Mr Ron Hunter and Mr John Currie (Napier University); Dr Stephen Ward-Smith and Mr Jason Dalby (Malvern Instruments Ltd); Mr Jimmy Robinson (Pixoft); Mr Bill Kerray (George Brown Engineering); Mr Dave Archer (Global Fluid Power); Dr Andrew Caswell (Wavin Plastics Ltd) and Mr Bill McTaggart (Brüel & Kjær).

7 REFERENCES

1. Fairfield C.A., Campbell S.A. & Reid D.B. Erosion performance of plastic pipes. Proc. 12th Int. Conf. Plastics Pipes, Baveno, Italy. (2004).
2. Campbell S.A. & Fairfield C.A. Damage assessment in plastic pipes by scanning electron microscopy. Proc. 12th Int. Conf. Plastics Pipes, Baveno, Italy. (2004).
3. Fairfield C.A. & Campbell S.A. Water jetting in clay and concrete sewers: a new angle on an old debate. Proc. 17th Int. Conf. Water Jetting, Mainz, Germany. 171-181 (2004).
4. Kobayashi K., Ito Y. & Oba R. Unsteady behaviour of cavity boundary directly related to cavity discharge. Proc. 17th Int. Conf. Water Jetting, Mainz, Germany. 317-326 (2004).
5. Soyama H., Yanauchi Y., Sato K., Ikohagi T., Oba R. & Oshima R. High-speed observations of ultrahigh-speed submerged water jets. J. Exp. Thermal Fluid Sci. **12** 411-416 (1996).

6. Matula T.J. Inertial cavitation and single-bubble sonoluminescence. Phil. Trans. Roy. Soc., Part A. **357** 225-249 (1999).
7. Blake J.R., Hooton M.C., Robinson P.B. & Tong R.P. Collapsing cavities, toroidal bubbles and jet impact. Phil. Trans. Roy. Soc., Part A. **355** 537-550 (1997).
8. Bourne N.K., Obara T. & Field J.E. High-speed photography and stress gauge studies of jet impact upon surfaces. Phil. Trans. Roy. Soc., Part A. **355** 607-623 (1997).
9. Summers D.A. & Wood B. Safety considerations in the use of high-pressure equipment. In; Labus T.J. & Savanick G.A. An overview of waterjet fundamentals and applications. 5th ed., Section 10, St Louis, Missouri, U.S.A. (2001).
10. Block, R.K. Bremsstrahlung. [http://rd11.web.cern.ch/RD11/rkb/PH14pp/node 16.html](http://rd11.web.cern.ch/RD11/rkb/PH14pp/node%2016.html) Organisation Européenne pour la Recherche Nucléaire (9 April 1998).

8 NOMENCLATURE

F {f(t)}	Fast Fourier transform
f_0	First fundamental frequency
T	Period of a function
t	Time
w	Weighting function
Q	Volumetric flow rate
ω	Angular velocity

Table 1 Comparison between the first fundamental frequency of the measured pressure fluctuations and the first fundamental frequencies of vibration of the pumphead and nozzle.

Target pressure/ psi	Target pressure/ MPa	$f_{o \text{ (pressure fluctuation)}}$ / Hz	$f_{o \text{ (pumphead)}}$ / Hz	$f_{o \text{ (nozzle)}}$ / Hz
2000	13.9	3.25	80.34	23.44
4000	27.6	2.25	80.94	58.59
6000	41.4	4.25	96.25	55.78
8000	55.2	4.00	N/A	311.6
10000	69.0	2.75	N/A	18.59

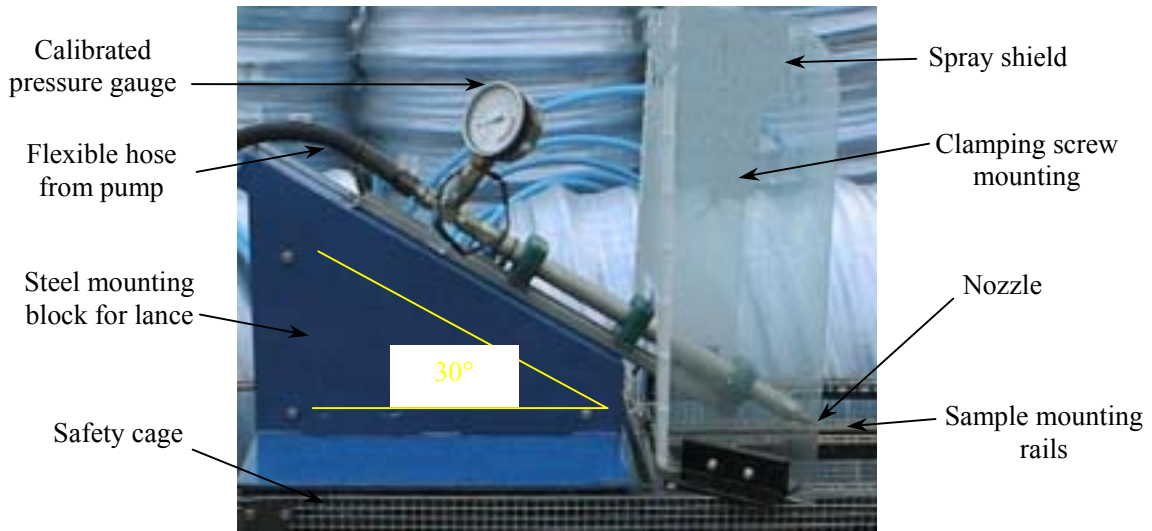


Figure 1 The test rig.

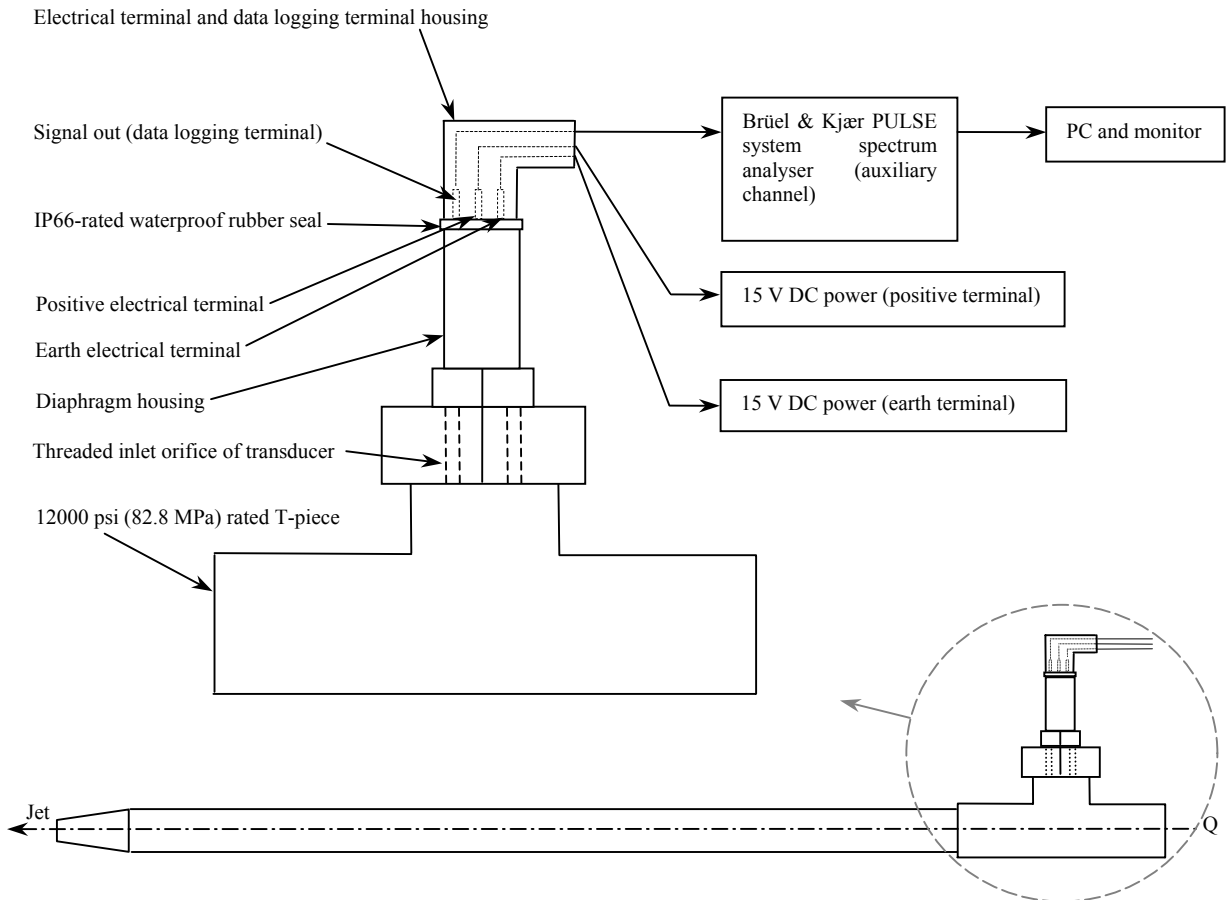


Figure 2 Schematic view of pressure transducer set-up.

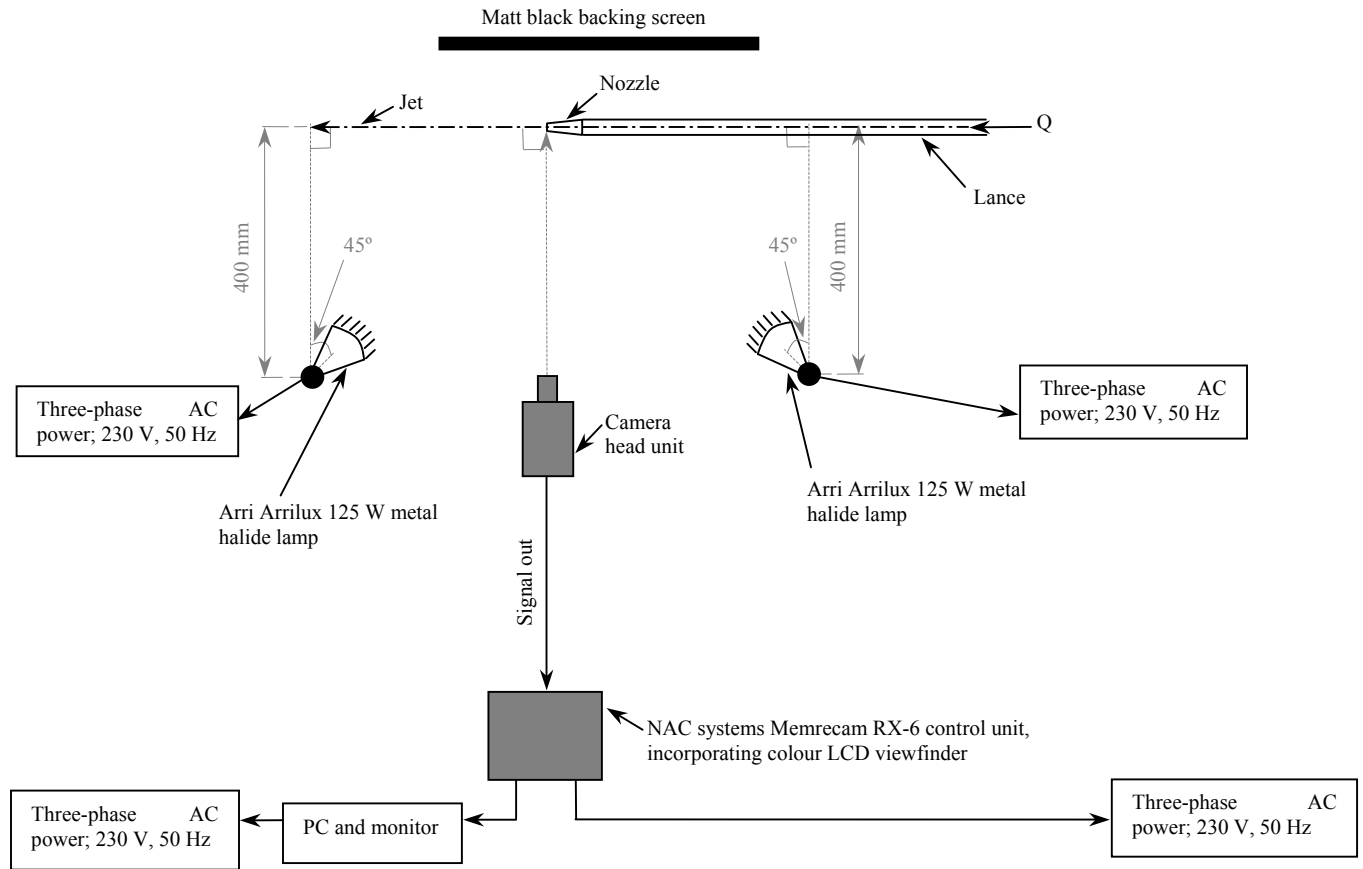


Figure 3 Schematic plan view of the high-speed video imaging set-up.



Figure 4 Series of stills taken from the high-speed video imaging of the jet running at 6000 psi (41.1 MPa); the interval between images is 5×10^{-5} s.

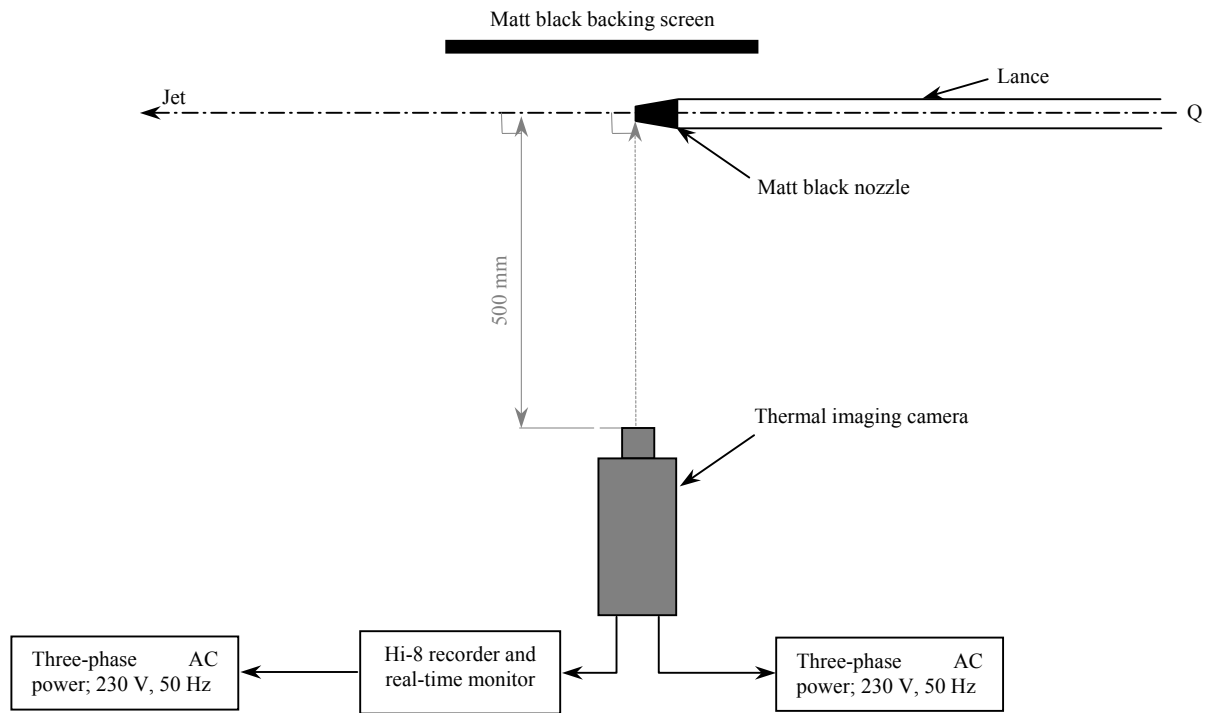


Figure 5 Schematic plan view of the thermal imaging set-up.

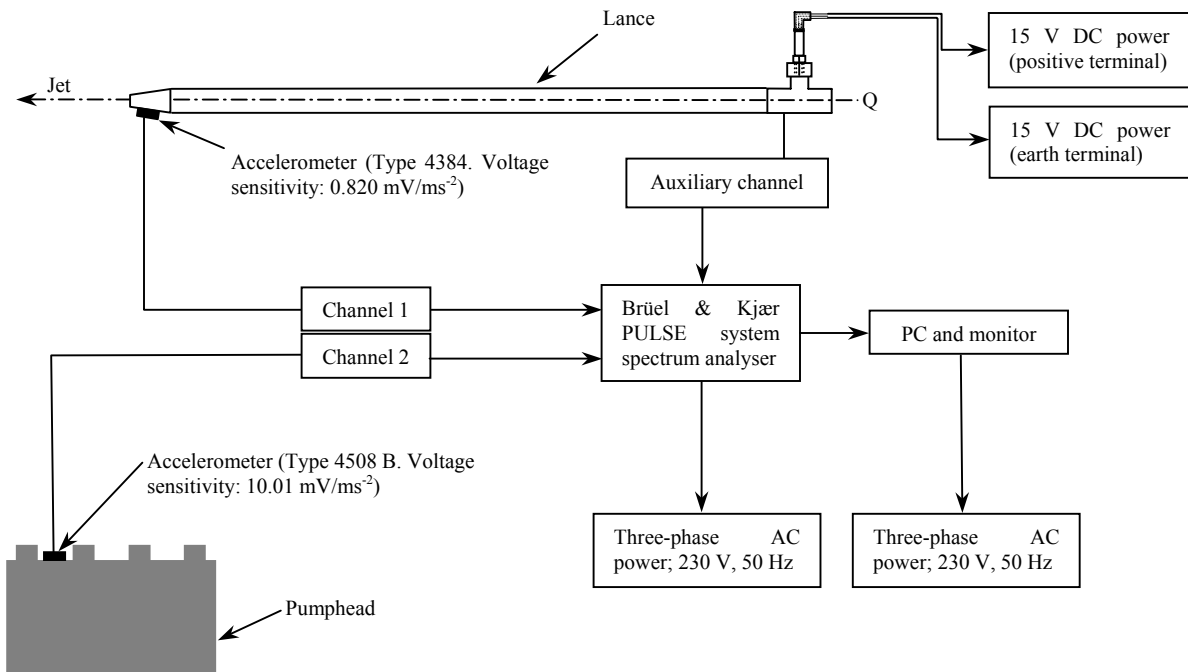


Figure 6 Schematic of the spectral analysis set-up.

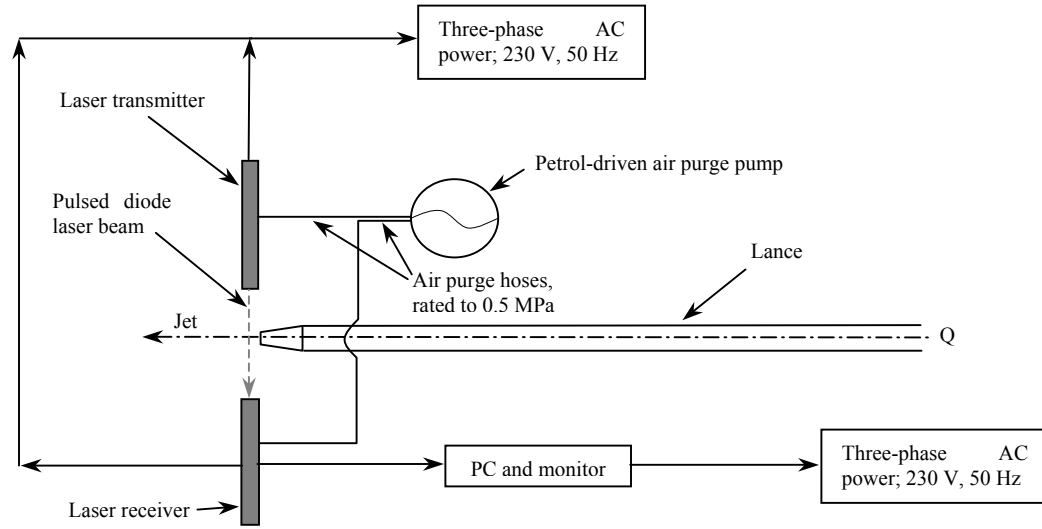


Figure 7 Schematic plan view of the Spraytec particle sizing set-up

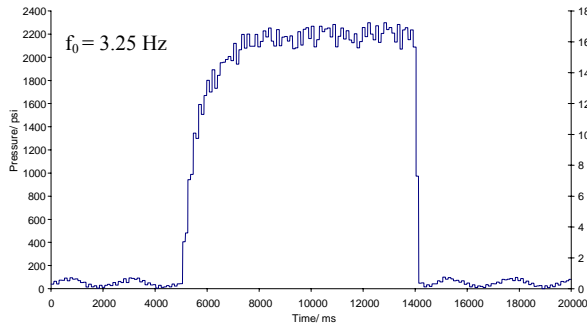


Figure 8 Pressure versus time plot for 2000 psi (13.8 MPa).

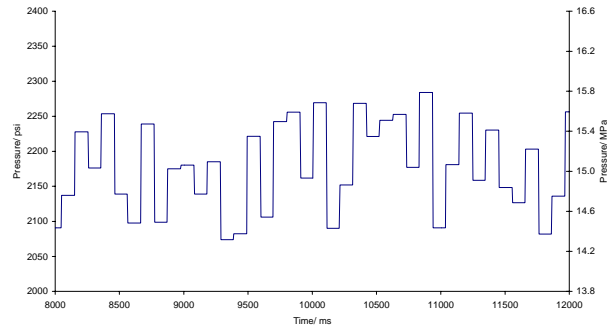


Figure 9 8000 ms to 12000 ms window of Figure 8.

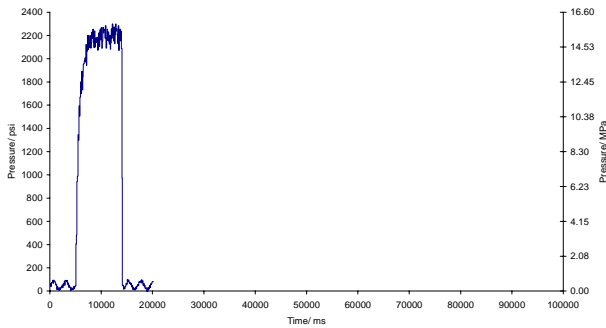


Figure 10 Extended window of Figure 8; up to 100000 ms.

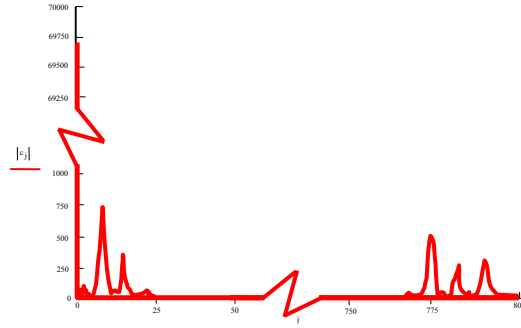


Figure 11 FFT output of Figure 8.

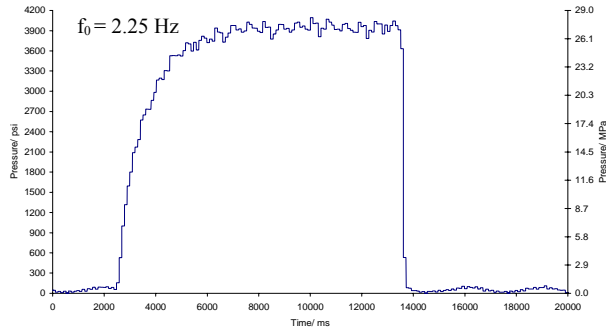


Figure 12 Pressure versus time plot for 4000 psi (27.6 MPa).

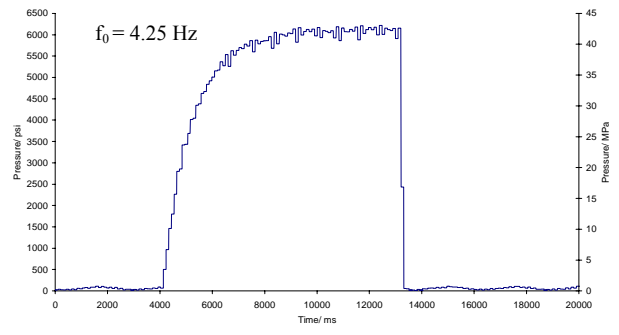


Figure 13 Pressure versus time plot for 6000 psi (41.4 MPa).

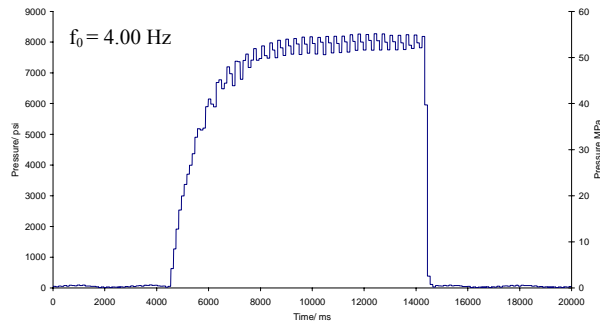


Figure 14 Pressure versus time plot for 8000 psi (55.2 MPa).

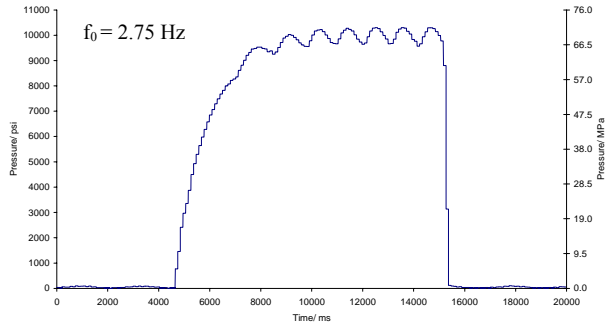


Figure 15 Pressure versus time plot for 10000 psi (69.0 MPa).

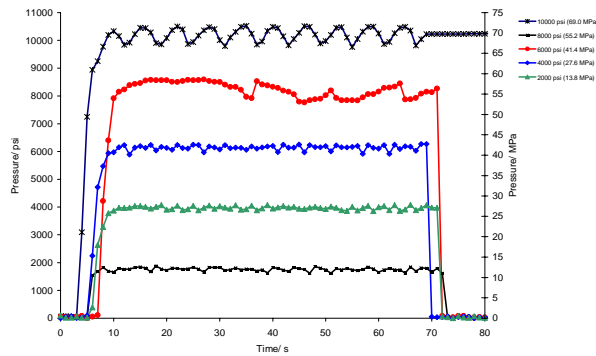


Figure 16 Combination of the fluctuations of all target pressures for a sampling rate of 1 s.

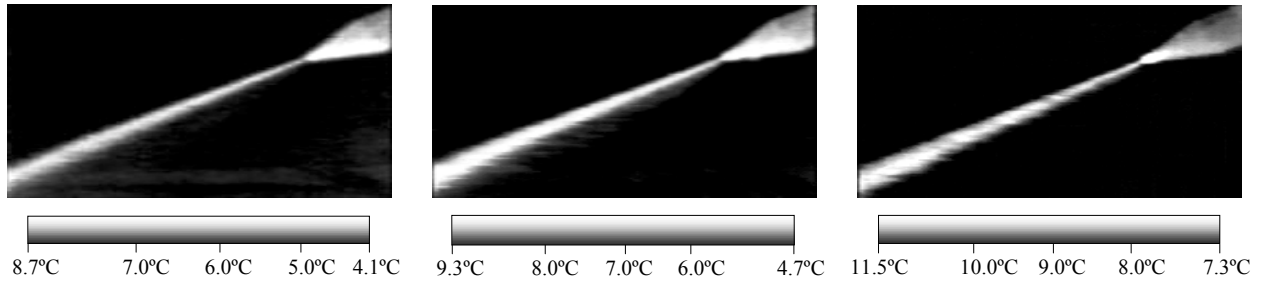


Figure 17 Still images taken from the thermal imaging footage. From left to right: 2000 psi (13.8 MPa) after one minute, 6000 psi (41.4 MPa), after one minute and 10000 psi (69.0 MPa) after one minute. The temperature range on each legend covers the maximum and minimum values on each frame.

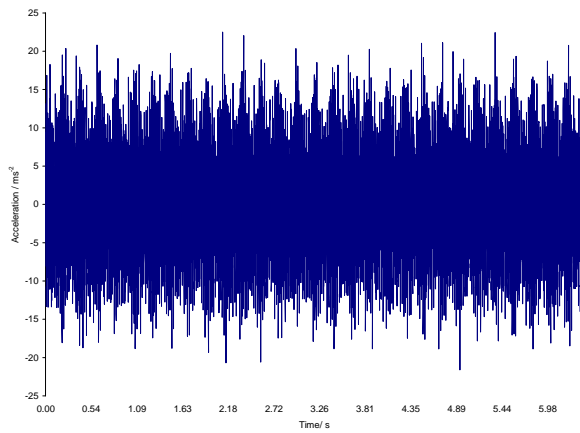


Figure 18 Time domain plot of the pumphead at 6000 psi (41.4 MPa).

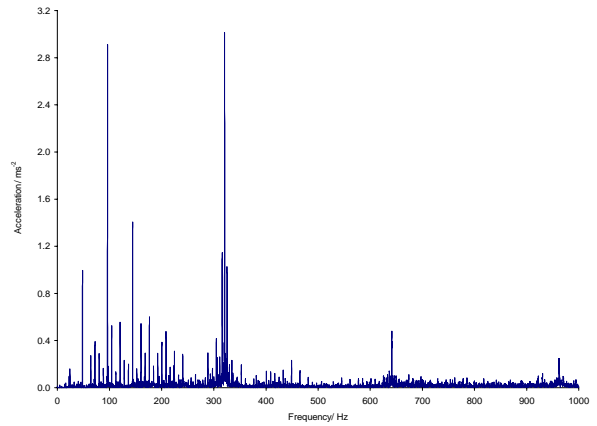


Figure 19 Resulting frequency domain plot of the pumphead at 6000 psi (41.4 MPa).

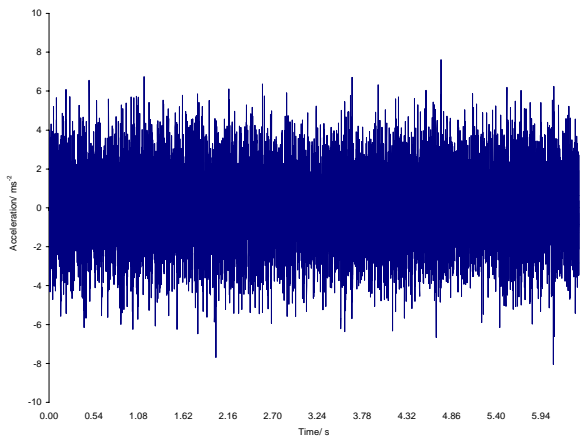


Figure 20 Time domain plot of the nozzle at 6000 psi (41.4 MPa).

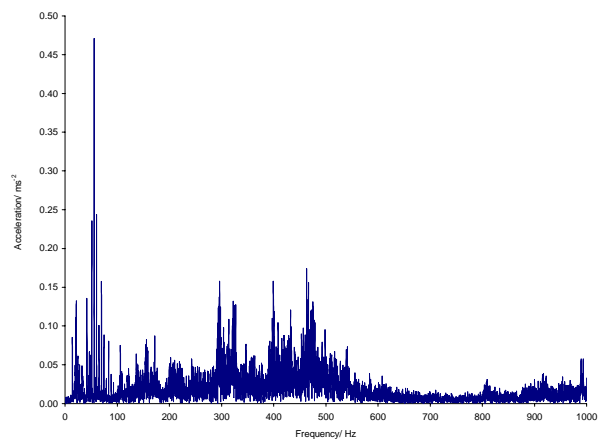


Figure 21 Resulting frequency domain plot of the nozzle at 6000 psi (41.4 MPa).

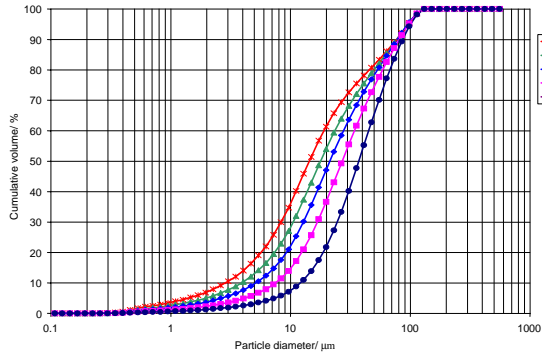


Figure 22 Cumulative volume grading curves for bubble diameters for target pressures.

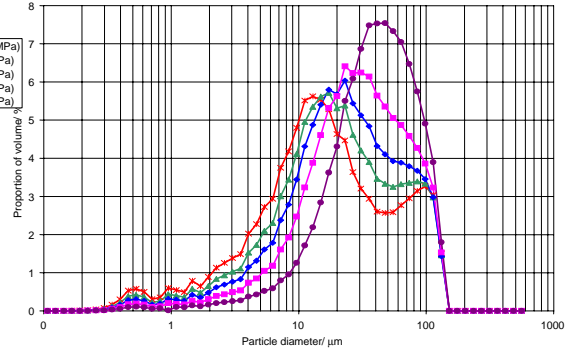


Figure 23 Bubble diameter proportions for all bubble diameters for target pressures.